Available online at www.sciencedirect.com

ScienceDirect

journal homepage: http://www.elsevier.com/locate/acme

Original Research Article

Experimental and analytical investigation on strengthening of heat damaged concrete by textile reinforced concrete (TRC)

J. Esmaeili *, *I. Sharifi*, *J. Kasaei*, *M. Nourizadeh*, *A. Ebrahimi Emamieh*

Department of Civil Engineering, University of Tabriz, 29 Bahman Boulevard, 51666 Tabriz, Iran

ARTICLE INFO

Article history:
Received 17 March 2019
Received in revised form
24 July 2019
Accepted 30 September 2019
Available online 30 October 2019

Keywords:
Textile reinforced concrete
Strengthening
Confinement
Elevated-Temperature
Confinement model

ABSTRACT

Composites fabricated of textile as reinforcement and a fine-grained concrete as matrix are referred to textile reinforced concrete (TRC) which provides the opportunity to build thin and shell constructions and to repair and strengthen concrete and masonry structures. This paper aimed to exploit the repair potential of TRC through confinement of heat-damaged concrete columns. For this purpose, a two-phase approach was conducted, in the first phase of which the effect of elevated temperature on mechanical properties of concrete was examined. The main objective of the second phase, however, was to assess the efficiency of glass textile reinforced concrete (GTRC) in the confinement of heat-damaged concrete. This phase commenced with selecting a candidate mortar among commonly used TRC mortars to confine heat-damaged specimens. Experimental results revealed that the adopted confinement system is an efficient solution to enhance the load bearing capacity of even seriously heat-damaged specimens. Eventually, experimental results were compared with available prediction models from the literature for both of the load-bearing capacity and also the compressive strength of confined concrete. Then an analytical confinement model was proposed based on best-fit analysis exclusive to heat-damaged concrete confined by GTRC.

1. Introduction

Existing concrete structures deteriorate over time and lose their expected performance due to some natural phenomena such as earthquake, fire, and chemical attacks. Reinforced concrete columns generally show appropriate performance during the fire, mainly due to the low thermal conductivity and incombustibility of the concrete cover maintaining the reinforcement and core concrete away from the destructive effects of fire. A concrete structure's collapse by fire seems improbable. Considering that such damages can be repaired in a majority of cases, the demolition or reconstruction of these structures is not economically, technically, and environmentally a sensible solution. Various methods have been proposed with the aim of repairing and strengthening existing concrete

* *Corresponding author.*
E-mail address: J-Esmaeili@tabrizu.ac.ir (J. Esmaeili).
https://doi.org/10.1016/j.acme.2019.09.008
1644-9665/

structures [1–4]. One of the most commonly used methods for strengthening purposes is exploiting FRP sheets to confine damaged concrete [5,6]. There are numbers of studies concerning the performance of heat-damaged columns wrapped by FRP [7–9]. Also, there is a growing interest toward investigating the effectiveness of FRP fabrics in strengthening and rehabilitation of chemically deteriorated concrete columns [10–12]. These studies confirm the efficiency of the FRP confinement technique in terms of enhancing the load-carrying capacity as well as increasing the ductility. The inclination toward utilizing FRP fabrics for strengthening and rehabilitation of damaged concrete is due to its low thermal conductivity, lightweight and appropriate performance as well as durability in the harsh environment [13,14]. This technique, however, entails some drawbacks, mostly inherited from its organic binder, such as: (1) poor performance at high temperatures above the glass transition temperature; (2) impossibility of application on wet surfaces; (3) high cost of material, labor, and application; and (4) incompatibility of the binder and substrate concrete. As an alternative to FRP, textile-reinforced concrete abbreviated as TRC has continued to gain acceptance in the civil engineering society addressing the problems associated with FRP. TRC is a novel composite material, which consists of woven yarns made of high strength material such as AR-glass, carbon, or basalt coupled with a high-performance fine-grained matrix [15,16]. Numerous studies have been conducted on the stress-strain behavior of TRC under tensile loading [17–20]. Also, flexural strengthening of RC beams with TRC as well as shear strengthening has always attracted the attention of researchers in this field [21–24]. In addition, a large number of studies have been carried out on TRC, as an innovative composite material for repairing and strengthening the concrete columns. The application of TRC for confining concrete columns was investigated by Triantafillou et al. [25]. They concluded that TRC contributes to the enhancement of load-bearing capacity and deformability through confinement. A Comparative study of TRC-confined and FRP-wrapped specimens was undertaken by Peled [26] and revealed that the TRC strengthening method significantly improved the modulus of elasticity in damaged concrete, compared to the FRP technique. Ortlepp et al. [27] studied the effect of cross-sectional geometry on the concrete columns confined with carbon and AR-glass textile. Basalt textile was also exploited by Garcia et al. [28] and Ludovico et al. [29] to confine concrete cylinders. Basalo et al. [30] investigated the confinement efficiency through different configurations of reinforcement material type and mortars. Ombres and Mazzuca [31] analyzed the collected results of compression tests carried out on concrete specimens confined by the fabric-reinforced cementitious matrix and proposed a prediction model for peak strength and corresponding strain of FRCM-wrapped specimens. Ortlepp et al. [32] assessed the applicability of TRC confining method for strengthening the structural RC columns and confirmed the practicality of strengthening RC columns by TRC. Since there are limited experimental and analytical investigations on the behavior of heat-damaged concrete confined with TRC, this study aims to improve the knowledge about the efficiency of this technique in strengthening of heat-damaged concrete.

2. Experimental program

2.1. Experimental design and objectives

This study aimed to evaluate the TRC confinement method for strengthening the heat-damaged concrete. To this end, a two-phase experimental approach was developed. In the first phase, the effects of elevated temperature on the concrete specimens were investigated to identify the characteristics of the heat-damaged concrete. Three different regimes of elevated temperature (300, 500, and 650 °C) beside the ambient temperature were considered. Then the most important mechanical properties such as compressive strength, modulus of elasticity, strain at peak stress, and stress-strain behavior of the heat-damaged concrete were taken into account, and the experimental results were verified using some available numerical models. All measures in the first phase were taken not only to obtain a better understanding of the effects of elevated temperature on the concrete behavior but also to investigate the confinement effect more reliably, which is the main objective of the second phase. The second phase of this study initiated with selecting a candidate mortar from different conventional TRC mortars to be used in the confinement of heat-damaged specimens. The selection was on the basis of confining performance, by assessing ultimate tensile strength through the uniaxial tensile test; and the applicability, by considering the workability and ease of application of mortar on the concrete cylinders. After determining the mortar, cylindrical specimens of each temperature regimes were confined by one or two layers of textile. These specimens, along with the unconfined heat-damaged ones were tested under the uniaxial compression, and the following parameters were investigated.

- Compressive strength enhancement imposed by confinement (f'_{ccT}/f'_{coT});
- Repairing capability determined by repair index ;
- Stress-strain behavior and relevant parameters such as elastic modulus, axial strain, and hoop strain.

The present study also aimed to discuss the existing models for TRC-confined concrete and to assess the potential of these models to predict the strength enhancement of heat-damaged concrete imposed by AR-glass textile-reinforced concrete (GTRC) confinement. Furthermore, an analytical model was proposed exclusively for GTRC-confined heat-damaged concrete.

2.2. Properties of textile material

In this study, the biaxial textile sheets made of multifilament yarns were used as reinforcement of fine-grained concrete, the fibers of which are made of alkali-resistant glass (Fig. 1). The properties of the textiles used in this study, which are commercially available and produced by the Solidian Company in Germany, are presented in Table 1. The mechanical properties of the textile were experimentally determined through tensile tests, by considering the ASTM D3039 [33] specifications, on the 400 mm length and 80 mm (containing seven yarns) width samples in both longitudinal and transverse direction. The diagrams obtained from the tests on

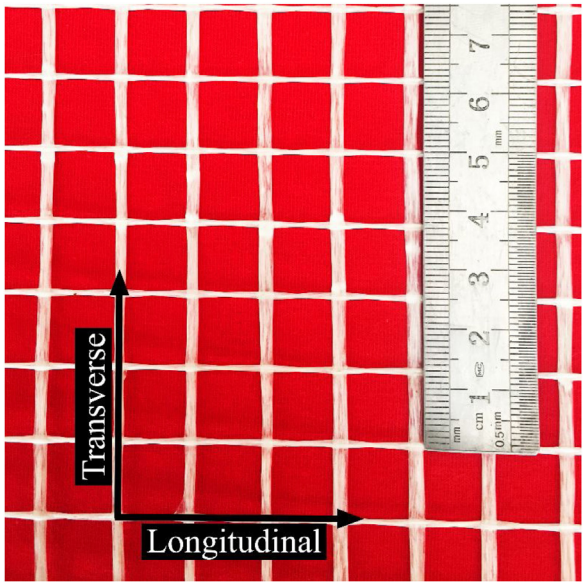

Fig. 1 – AR-Glass textile fabric.

samples with one and two layers of the textile are illustrated in Fig. 2, and the mean test results are represented in Table 1.

2.3. *Properties of Mortars*

The maximum size of aggregates used in the present study was 1 mm. Portland Cement CEM I 42.5 R (according to European standard EN 197-1 [34]), fly ash, silica fume, water, and also poly-carboxylate based liquid hyper-plasticizer with a specific gravity of $1.11 \pm 0.05\, g/cm^3$ were used for preparing mortars. The chemical analysis and also some physical properties of Portland cement, fly ash, and silica fume are represented in Table 2.

The degree of alkalinity of the matrix plays an important role in the matrix selection. The alkalinity of the matrix results in the decomposition of the embedded glass filaments. Hence matrixes with a binder containing the low content of Portland cement are preferred. In this study, three types of commonly used mortars in the case of TRC within the framework of the Collaborative Research Centers 528 at the TU Dresden and Collaborative Research Center 532 at RWTH Aachen, were adjusted by available materials and used to produce tensile specimens [35–37]. Table 3 presents the mix design and compressive strength test results of these mortars, according to ASTM C 109 [38]. The flow-table test was carried out on all mortar mixes in conformity with ASTM C 230 [39]. The table flow spread of 180–200 mm was kept constant for all types of mortars by adjusting the hyper-plasticizer dosage.

2.4. *Casting of specimens and testing procedure*

2.4.1. *Tensile composite specimens*

In order to conduct a direct tensile test and to investigate the stress-strain behavior of TRC, nine flat rectangular specimens of 400 mm length, 80 mm width, and 6 mm thickness of three different mortars were prepared (Fig. 3a). The ratio of 1/5 (width/height) seemed appropriate to limit the Poisson effect [20]. To cast these specimens, two layers of textile were arranged and fixed at the ends of the mold as can be seen in Fig. 3a in detail. The casted specimens were kept in a steam chamber with a temperature of 25 ± 1°C for a day to prevent the formation of early-age cracks. Then the specimens were cured for 90 days in a water tank with a temperature of 23 ± 1 °C. After 90 days; the holes were created at both ends of the test specimens along their central longitudinal axis. Steel plates with a thickness of 4 mm were bonded at the two ends of the specimens using epoxy resin for appropriate force transition during the tensile test. The hinge mechanism, the details of which are shown in Fig. 3b was used to eliminate the bending moment formation. Specimens were subjected to direct tensile test using a displacement-controlled hydraulic jack at a rate of 0.5 mm/min. Displacements were measured by means of two linear variable differential transformers (LVDTs) along the 200-mm measurement length on both sides of the specimens in the longitudinal direction (Fig. 3c). All data was compiled by a data acquisition system at a frequency of 10 Hz.

2.4.2. *Cylindrical specimens and heating regimes*

Cylindrical specimens were cast with a diameter of 100 mm and a height of 200 mm. The specimens were stored in a water tank with a temperature of 23 ± 1 for 28 days and for 62 days in the laboratory at the ambient temperature to become 90 days old. Then the specimens were divided into four

Table 1 – Characteristics of AR-glass textile.

Manufacturer given data			
Product name	GRID Q20/20-AAS-13		
Fiber material	Alkaline Resistance glass		
Center distance of yarns	Longitudinal and transverse	(mm)	13
Fiber cross-section area of yarns	Longitudinal and transverse	(mm^2)	0.25
Cross-section area of textile	Longitudinal and transverse	(mm^2/m)	20
Tensile strength (characteristic value)	Longitudinal	(MPa)	1200
	Transverse	(MPa)	1300
Experimental results			
Average ultimate tensile Strength ± SD	Longitudinal	(MPa)	825 ± 24.3
	Transverse	(MPa)	962 ± 26.3
Average ultimate tensile strain ± SD	Longitudinal	(%)	2.5 ± 0.12
	Transverse	(%)	1.9 ± 0.08
Average Young's modulus ± SD	Longitudinal	(GPa)	31 ± 1.28
	Transverse	(GPa)	50.7 ± 1.45

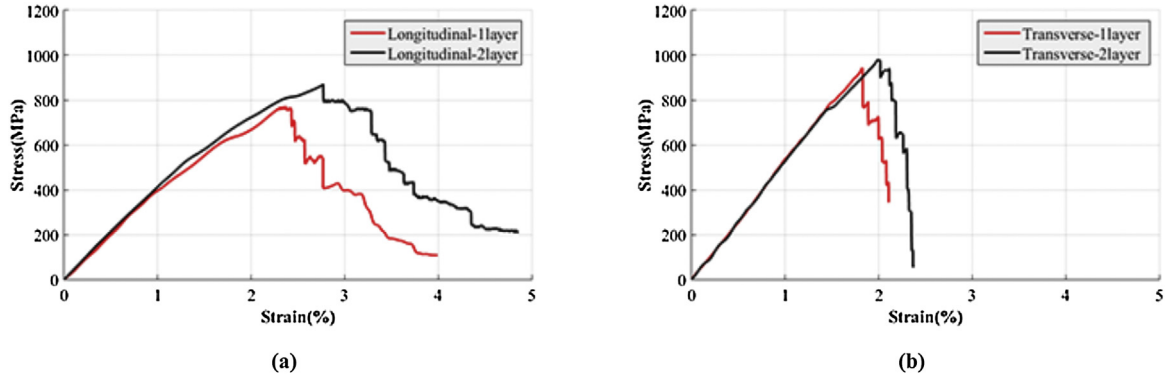

Fig. 2 – Stress-strain curves of AR-glass textile derived from direct tensile test. (a) longitudinal direction. (b) transverse direction.

Table 2 – Physical properties and chemical composition of cement, fly ash, and silica fume.

Component	SiO_2	Al_2O_3	Fe_2O_3	CaO	MgO	Na_2O	K_2O	SO_3	L.O.I[a]	Specific gravity	Blaine fineness (m^2/kg)
OPC (%)	21.57	4.65	3.03	63.32	2.40	0.32	0.81	ND[b]	1.33	3.05	382
Fly Ash (%)	44.93	26.17	9.20	5.66	1.83	2.62	2.15	3.22	3.26	2.44	325
Silica Fume (%)	89.22	1.20	2.12	1.87	1.61	0.55	1.05	ND	2.60	2.20	541

[a] Loss of Ignition (1000**x2103;**).
[b] Not Detected ($<0.01\%$).

Table 3 – Mix design and compressive strength of mortars.

Mix No	Cement $\left(\frac{kg}{m^3}\right)$	Fly ash $\left(\frac{kg}{m^3}\right)$	Silica fume $\left(\frac{kg}{m^3}\right)$	w/b	Water $\left(\frac{kg}{m^3}\right)$	Sand $\left(\frac{kg}{m^3}\right)$	Hyper plasticizer $\left(\frac{kg}{m^3}\right)$	Compressive strength ± SD[a] (MPa)
PZ-0899-01	490	175	35	0.4	280	715	4	63 ± 1.8
M3	549	246	25	0.3	246	1092	5.5	75 ± 2.6
M7	839	—	—	0.33	277	1189	5	80 ± 1.4

[a] Average compressive strength of six 5 × 5 × 5 cm cubic specimens at 28 days age.

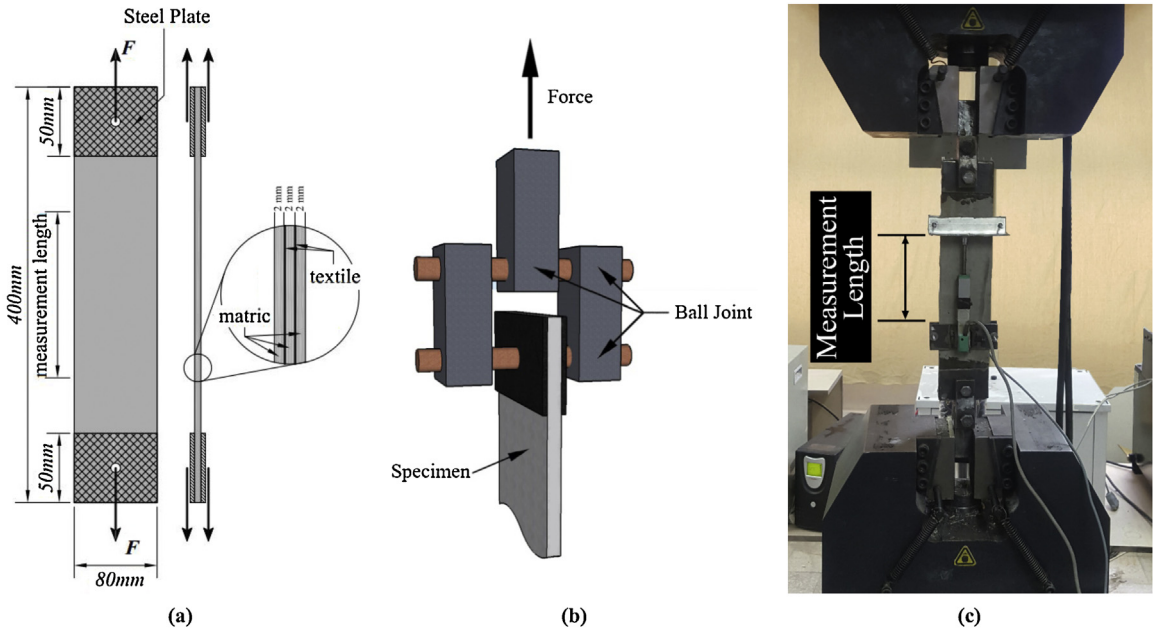

Fig. 3 – (a) tensile specimen geometry; (b) hinged mechanism; (c) direct tensile test setup.

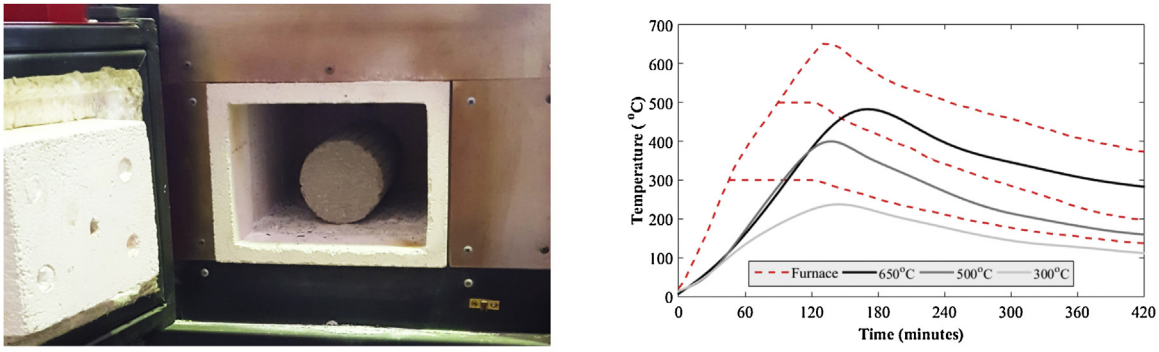

Fig. 4 – (a) furnace with cylindrical concrete specimen; (b) typical temperature records of furnace and specimens' core.

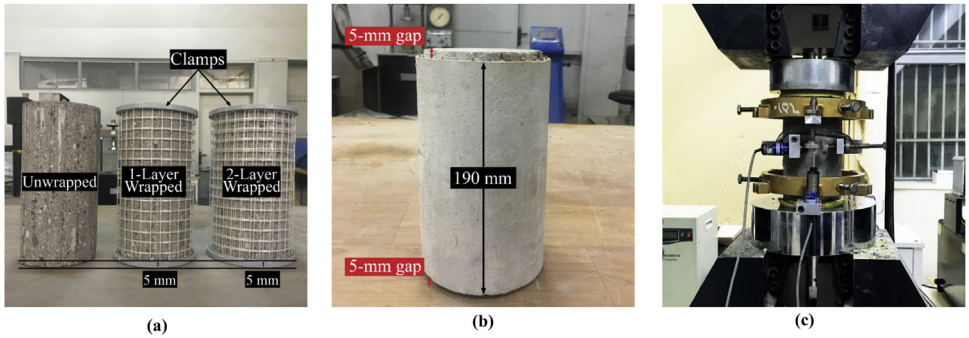

Fig. 5 – (a) unwrapped and wrapped specimens with AR-Glass textile; (b) confined specimen; (c)compression test setup.

groups, each containing nine specimens from the same batch. The first group of nine specimens was kept in the ambient condition in the laboratory, and the other three groups were exposed to different regimes of elevated temperature including 300 ℃, 500 ℃, and 650 ℃ in an electrical furnace (Fig. 4 a). The reason for selecting these regimes of elevated temperature lies in two following facts: (I) in similar studies and codes, the reported temperatures which cause a considerable loss in the mechanical properties of concrete structures, is above 300℃; (II) damaged concrete structures should be in a state that the strengthening procedure will be practically justifiable. As the similar studies stated, the damages that concrete structures experiences in temperatures below 700℃, could be strengthened and retrofitted practically [7,40,41]. Moreover, the duration of heating scenario was considered 120 min, which is representative of fire resistance duration of tall buildings according to UK Building regulations [42].

The temperature of concrete's core was measured during the heating process using K-type thermocouples. The furnace was scheduled to heat the specimens to target temperature with a maximum rate and then to hold that temperature. When the total heating time had reached 120 min, the furnace was turned off, and specimens were allowed to be cooled down gradually. The typical temperature records are presented in Fig. 4b. This figure depicts the temperature of the concrete core as well as the temperature inside the electrical furnace for different temperature regimes.

2.4.3. Strengthening procedure and experimental test setup

For the better bonding of the mortar to the substrate concrete, surface grinding operations were carried out on specimen. For this purpose, a series of grooves were created in a parallel orientation to the height axis of the unwrapped cylinders and about 2 cm apart from each other (Fig. 5a). Then the specimens were cleaned using the water jet. Eventually, the following steps were performed to confine the specimens with one or two layers of textile: 1) Surface of the all specimens were dampened to improve the bonding between mortar and substrate concrete; 2) As illustrated in Fig. 5a, textile sheets were kept straight between a pair of 2-mm thickness clamps installed on top and bottom of the specimens to hold textile sheets at the exact distance of 2 mm from the specimen and outer side of the applied mortar. For one-layer specimens, total mortar thickness was approximately 5 mm with a textile sheet in the center, and the mortar thickness for two-layer specimens was approximately 7 mm with two textile layers arranged uniformly at a distance of 2 mm from each other. As shown in Fig. 5b, the 5-mm gaps were considered on both ends of the specimens to eliminate the potential axial load on the TRC jacket during the tests. Moreover, an overlap of 12 cm was considered for each layer; 3) Hand lay-up application was undertaken to impregnate the textile fabrics by mortar; 4) A metallic trowel was used to smoothen the exterior layer of confinement. To preclude cracking of the mortar caused by shrinkage, the confined specimens were kept in a steam chamber with a temperature of 25 ± 1 °C for one day after

removing clamps and then stored for 90 days in a water tank with a temperature of 23 ± 1 °C.

The confined specimens were tested by a displacement-control hydraulic jack for compressive strength with a controlled displacement rate of 0.5 mm/min (Fig. 5c) and their force-displacement diagrams were recorded using a data acquisition system at a frequency of 10 Hz according to ASTM C39 / C39M-16 [43] and ASTM C469 / C469M-14 [44]. The X-T-N template was used to tag the cylindrical specimens, where X indicates whether the specimens were wrapped or not with the dedication of the letter W for wrapped specimens and U for unwrapped ones. Furthermore, T demonstrates the thermal regimes of 20, 300, 500, and 650 °C to which the test specimens were exposed. Moreover, N shows the number of textile layers, which was one or two in the present research.

3. Experimental results and discussion

In this study, a two-phase approach was conducted to discuss the experimental results in detail. In the first phase, the unconfined concrete specimens were exposed to elevated temperature, and then their results were verified based on concrete mechanical properties models and relationships to obtain more reliable and confident results of experimental testing procedures. The second phase specifically argues on the confinement effects of the TRC strengthening technique, and a prediction model was eventually taken into account. As a brief overview, the experimental key results are presented in Table 4 for the groups of different elevated temperatures, and different numbers of the textile layers applied on the specimens. The data includes peak stress, axial and hoop strain at peak stress, and elastic modulus.

3.1. *Effect of elevated temperature on mechanical properties of concrete (Phase I)*

This phase provides a comparison between the experimental observations and the existing models which are summarized in Appendix B in terms of compressive strength, elastic modulus, axial strain at peak stress, and stress-strain diagrams.

Several numerical models were selected from a vast majority of compressive strength models of concrete exposed to elevated temperature (Appendix B). Fig. 6a presents the four compressive strength prediction models beside experimental results to determine their potential coincidence. Based on Fig. 6a, as the elevated temperature increases the residual compressive strength of the concrete is reduced significantly, which is clearly in conformity with previous studies in the literature [45,46]. The difference between the thermal strain of the cementitious matrix and aggregates of the concrete triggers the formation of micro-cracks. As the temperature rises, at first, the hardened cement matrix begins to expand and then shrinks due to water loss. However, the concrete aggregates expand during the entire time of heating scenario [46,47]. These strain differences develop stresses among hardened cementitious matrix and aggregates, which causes the generation of micro-cracks in the interfacial transition zone (ITZ). These

Table 4 – Summary of experimental results.

Specimen group[a]	Target temperature (°C)	Number of layers	Peak stress ± SD (MPa)	Axial strain at peak stress ± SD (%)	Hoop strain at peak stress ± SD (%)	Elastic modulus ± SD (GPa)	$\left(f'_{cc}/f'_{co}\right)^{b}$	$\left(f'_{ccT}/f'_{coT}\right)^{b}$
U-20	Ambient	—	43.66 ± 1.7	0.24 ± 0.026	−0.11 ± 0.005	28.13 ± 2.31	1.00	—
W-20-1		1	46.81 ± 4.3	0.18 ± 0.012	−0.12 ± 0.017	30.61 ± 3.08	1.07	—
W-20-2		2	50.84 ± 1.5	0.17 ± 0.022	−0.28 ± 0.062	32.61 ± 2.66	1.16	—
U-300	300	—	36.87 ± 3.2	0.31 ± 0.017	−0.10 ± 0.021	16.45 ± 1.77	—	1.00
W-300-1		1	43.54 ± 2.7	0.28 ± 0.022	−0.47 ± 0.046	17.43 ± 3.16	—	1.18
W-300-2		2	49.26 ± 4.5	0.26 ± 0.029	−0.14 ± 0.009	19.70 ± 3.00	—	1.34
U-500	500	—	27.54 ± 2.0	0.51 ± 0.074	−0.35 ± 0.043	8.55 ± 1.31	—	1.00
W-500-1		1	35.53 ± 4.7	0.37 ± 0.045	−0.51 ± 0.081	8.89 ± 2.21	—	1.29
W-500-2		2	43.24 ± 2.7	0.30 ± 0.012	−0.68 ± 0.264	10.71 ± 1.23	—	1.57
U-650	650	—	18.61 ± 2.5	0.64 ± 0.065	−1.00 ± 0.176	4.68 ± 0.58	—	1.00
W-650-1		1	28.32 ± 2.9	0.40 ± 0.107	−1.24 ± 0.349	5.46 ± 0.79	—	1.52
W-650-2		2	40.58 ± 3.2	0.37 ± 0.066	−1.27 ± 0.242	8.31 ± 1.85	—	2.18

[a] Each group contains three specimens.
[b] Efficiency of confinement for the compressive strength.

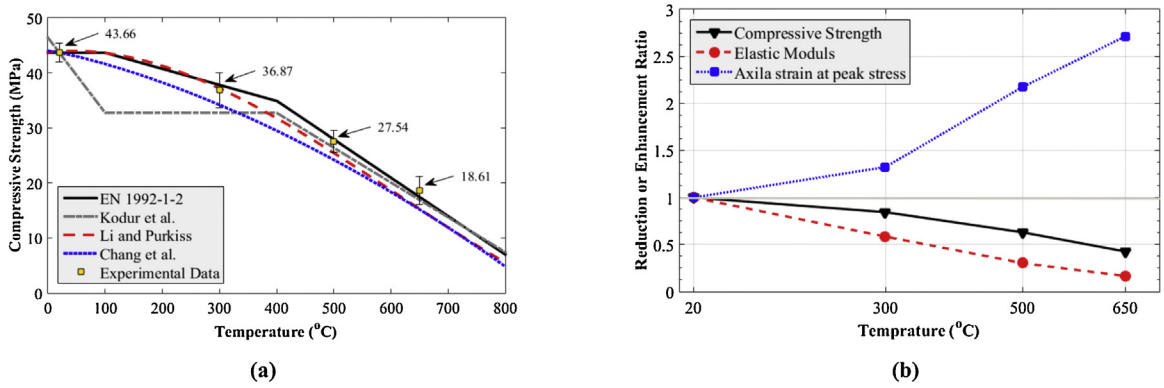

Fig. 6 – (a) experimental compressive strength results versus elevated temperature in comparison with existing prediction models; (b) reduction or enhancement ratios of mechanical properties of concrete specimens versus elevated temperature.

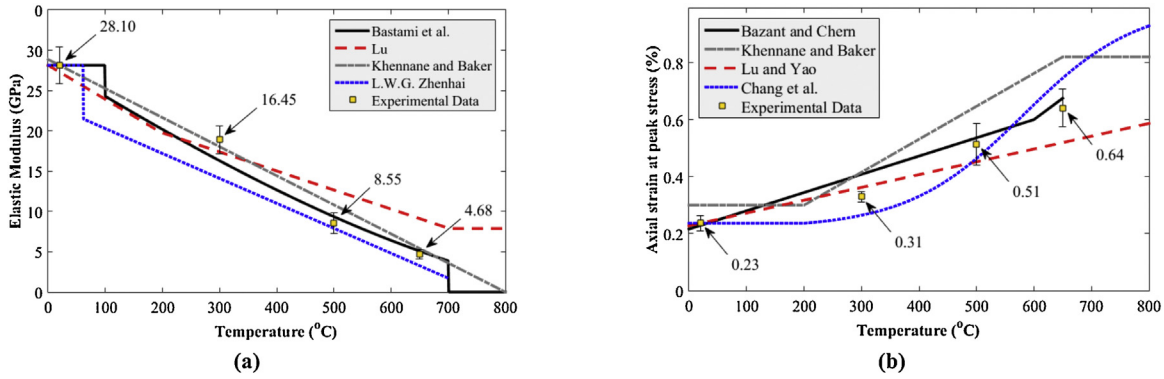

Fig. 7 – Effect of elevated temperature on (a) elastic modulus and (b) axial strain at peak stress of concrete for both of experimental data and existing prediction models.

micro-cracks account for the reduction of some mechanical properties of concrete, for instance, compressive strength at elevated temperature. Fig. 6b indicates the reduction ratio $\left(f'_{coT}/f'_{co}\right)$, where f'_{coT} is the compressive strength of concrete exposed to elevated temperature and f'_{co} is the compressive strength of concrete at ambient temperature. Notable reductions were observed in the specimens exposed to temperatures above 300 °C. Residual compressive strength of concrete exposed to elevated temperature could be interpreted by three stages [46]: (I) within 20 **x2103;** to 300 **x2103;**, Compressive strength of concrete remains constant or even experience a slight increase; (II) within 300 **x2103;** to 800 **x2103;**, compressive strength of concrete declines substantially; (III) 800 **x2103;** afterwards, approximately all the compressive strength of concrete has been lost. As can be seen in Fig. 6b, the reduction ratio related to 300, 500, and 650 °C is 0.84, 0.63, and 0.43, respectively.

Since the modulus of elasticity is directly proportional to compressive strength, the same decreasing trend in the compressive strength values was expected for the modulus of elasticity. Fig. 7a compares some important available numerical models for the elastic modulus of concrete exposed to elevated temperature, which are represented in Appendix B thoroughly. The experimental results of the elastic modulus are in agreement with those of the models' prediction (Fig. 7a). Fig. 6b shows that the elastic modulus reduction ratio (E_{cT}/E_c) is 0.58, 0.30, and 0.17 for the corresponding elevated temperatures of 300, 500, and 650 °C, respectively.

Strain values derived from numerical models exhibit generous scattering; nevertheless, experimental data sit within the predicted boundaries of numerical models, as shown in Fig. 7b. In contrast to the compressive strength and modulus of elasticity, the axial strain revealed an upward trend with an increase in the temperature, which could be attributed to the formation of the cracks caused by the incompatibility of aggregates and cement paste during heating exposure [48]. The ratio of the axial strain at peak stress of heat-damaged specimens to that of the unheated ones $(\epsilon_{cT}/\epsilon_c)$ is 1.32, 2.17, and 2.71 under regimes of 300, 500, and 650 °C, respectively (Fig. 6b).

Some of the important numerical stress-strain relationships for concrete exposed to elevated temperatures are summarized in Appendix B. Numerical, and experimental stress-strain curves are plotted in Fig. 8 for different regimes of elevated temperature. From Fig. 8, it can be noted that, as the temperature rises, the stress-strain curve becomes flatter, and the peak stress values move rightwards and downwards. Also comparing the experimental diagrams with the diagrams derived from models reveals the coincidence of the experimental and model curves, which verifies the accuracy of the laboratory results.

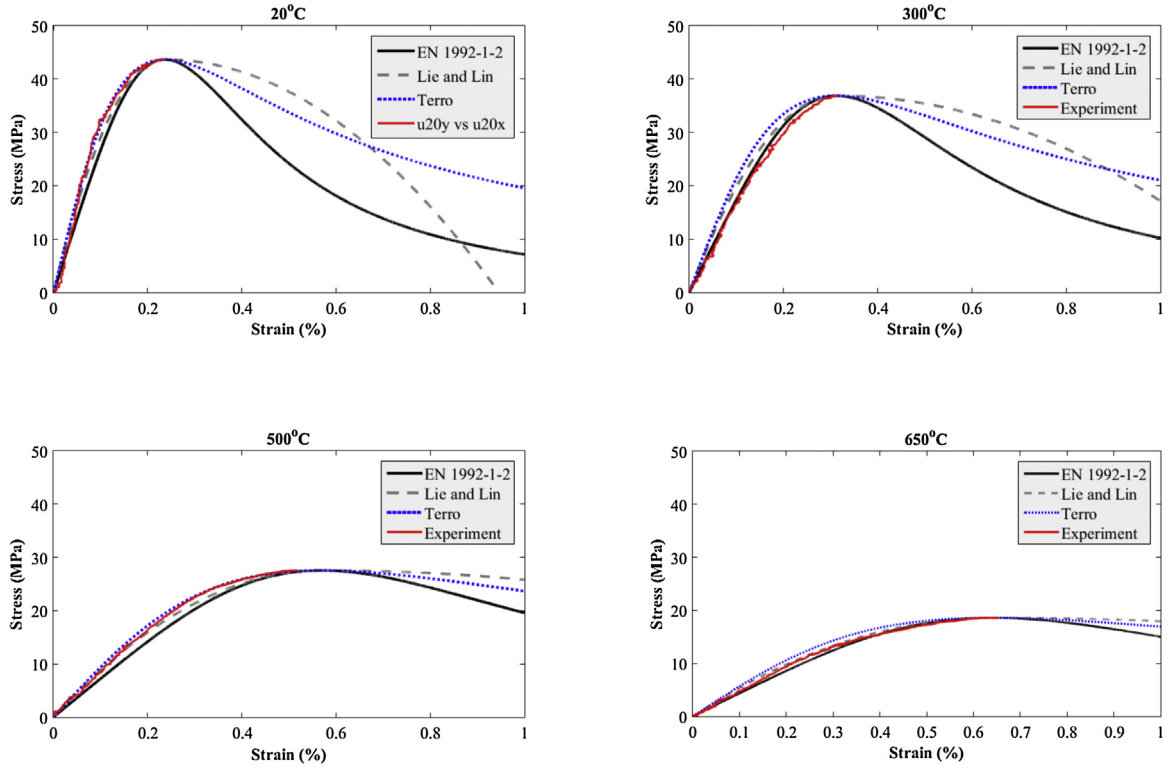

Fig. 8 – Comparison of experimental stress-strain curves with existing numerical models at different regimes of elevated temperature.

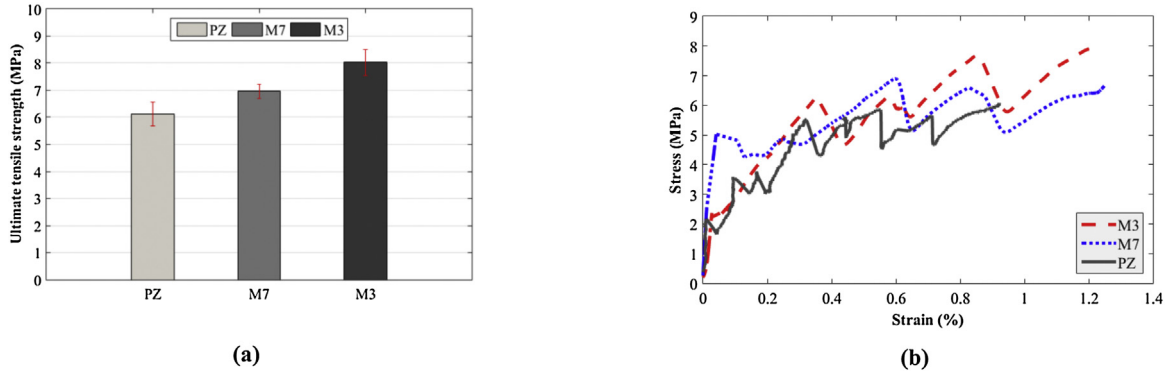

Fig. 9 – Mechanical properties of TRC: (a) ultimate tensile strength; (b) stress-strain behavior.

3.2. *Effect of TRC confinement on mechanical properties of heat-damaged concrete (Phase II)*

3.2.1. *TRC composite selection for confinement*

Under compression testing, lateral deformation of the cylindrical specimens develops tensile stresses within the TRC composite jacket. As a consequence, the higher the ultimate tensile strength of the TRC composite is, the higher the load-carrying capacity of confined specimens is expected. Three commonly used mortars (M3, M7, and PZ) were utilized to produce TRC composites, which were examined through the direct tensile test. Ultimate tensile strength and the stress-strain behavior of TRC composites made of these three aforementioned mortars are illustrated in Fig. 9. Eventually, the TRC composite produced by M3 mortar was preferred to confine cylindrical specimens with regard to its higher ultimate tensile stress, ease of application founded on empirical observations, and a lower degree of alkalinity which is mainly influenced by the amounts of Portland cement in the mixture. Besides, the ability of the matrix to impregnate textile meshes is an important factor which develops a proper bond between matrix and textile and also leads to a better redistribution of stresses within the composite material and then the maximum tensile capacity of the composite material could be attained.

3.2.2. *Confined concrete properties*

The results of the compression tests on confined specimens are reported in Table 4. The main mechanical properties of the heat-damaged concrete specimens confined by GTRC are discussed in

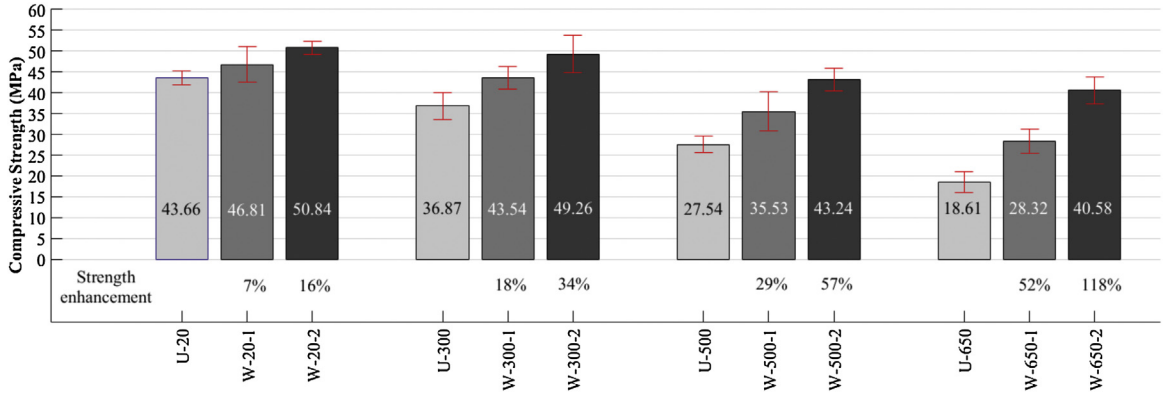

Fig. 10 – Comparison of compressive strength and the strength enhancement of specimens due to confinement at each temperature regime.

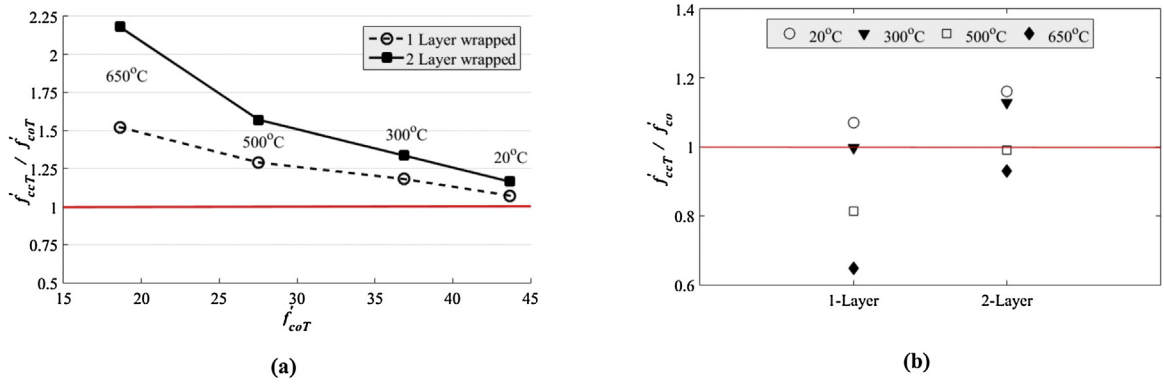

Fig. 11 – Confinement efficiency: (a) compressive strength enhancement and (b) repair index resulted by TRC confinement.

details for the peak stress, axial and hoop strains at peak stress, elastic modulus, and also the effectiveness of the confinement.

The compressive strengths of all confined heat-damaged cylindrical specimens are illustrated in Fig. 10. Moreover, the enhancement factor, as the ratio of confined concrete compressive strength to that of the corresponding unconfined specimen at each elevated temperature regime is presented in Fig. 10. Experimental results revealed that confinement has considerable effects on the improvement of compressive strength in all heat-damaged concrete specimens. It was clearly observed that the more reinforcement ratio (textile layers) is implemented in the TRC composite, the higher increase in compressive strength is obtained. Regarding the number of textile layers applied on cylindrical specimens, the enhancement ratio of approximately 7–118% was observed considering all temperature regimes.

As the compressive load increases in a confined compression member, the tensile stresses in the confining system arises due to the lateral deformations of the specimen. By arising the tensile stress in composite material and because of the poor tensile strength of the fine-grained concrete, the cracks appear on the outer sides of the confining jacket and will continue to the inner part. As the more cracks appears and getting wider, the bonds between the mortar and textile become weaker. Eventually, the failure of the specimen occurs with the failure of the confining jacket.

It is also worth noting that the effect of confinement on compressive strength enhancement of heat-damaged specimens is much more remarkable when the specimens are exposed to higher regimes of elevated temperature. Generally, the confining method is more efficient for strengthening of the concrete with lower compressive strength which is in conformity with the results of available research in the literature [25,49,50]. As it can be seen in Fig. 10, a maximum compressive strength enhancement of 118% was observed in W-650-2.

Another noteworthy point to consider is the capability of the TRC confinement method in compensating the specimens' strength loss imposed by elevated temperature. The efficiency of the confinement in the case of compressive strength for each of the temperature regimes is defined as f'_{ccT}/f'_{coT}, where f'_{ccT} is the compressive strength of confined specimens and f'_{coT} is the compressive strength of unconfined specimens. The mentioned confinement efficiency (f'_{ccT}/f'_{coT}) is plotted against f'_{coT} in Fig. 11a. It can be noticed that the TRC confinement technique is more efficient as the elevated temperature rises considerably.

In Fig. 11b, the ratio of the compressive strength of confined heat-damaged specimens (f'_{ccT}) to the compressive strength of the specimen U-20 (f'_{co}) is defined as repair index indicating the rate of strength loss compensation. The repair operation is considered as a successful technique when the value of repair index tends to one ($f'_{ccT}/f'_{co} \approx 1$). In fact, the values below one imply the imperfection of the strength loss compensation. In

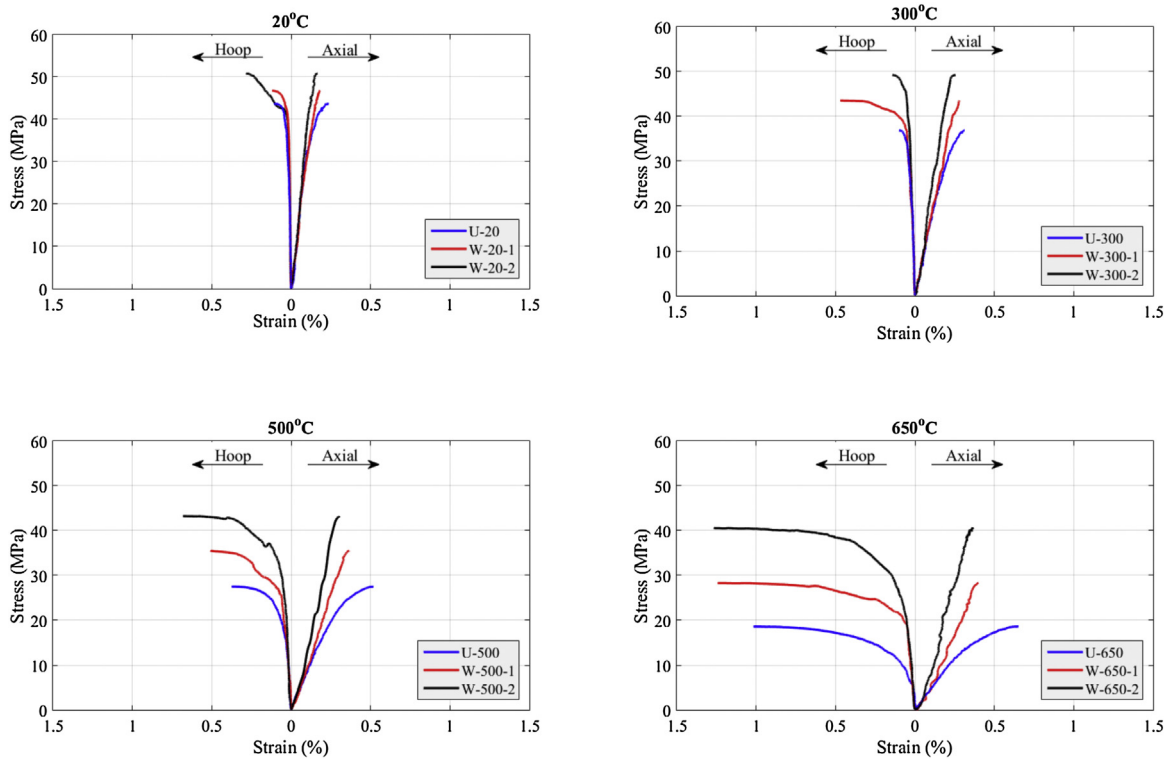

Fig. 12 – Stress versus axial and hoop strains diagrams at different regimes of elevated temperature.

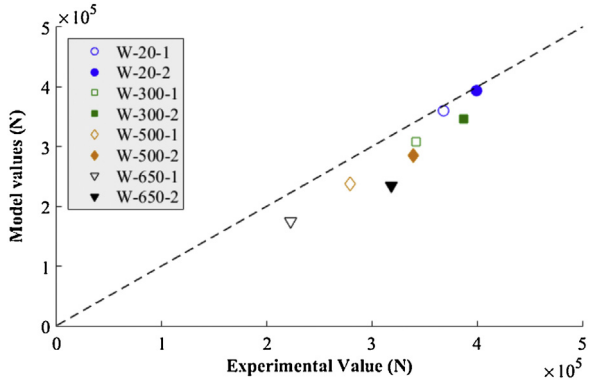

Fig. 13 – Ultimate load capacity comparison between experimental data and model predictions.

Table 5 – Existing prediction models.

Model	Analytical expressions
Ombres and Mazzuca	$\frac{f'_{cc}}{f'_{co}} = 1 + 0.913\left(\frac{\sigma_{lu}}{f'_{co}}\right)^{0.5}$
Triantafillou et al.	$\frac{f'_{cc}}{f'_{co}} = 1 + 1.9\frac{\sigma_{lu}}{f'_{co}}$
De Caso et al.	$\frac{f'_{cc}}{f'_{co}} = 1 + 2.87\left(\frac{\sigma_{lu}}{f'_{co}}\right)^{0.775}$
ACI	$\frac{f'_{cc}}{f'_{co}} = 1 + 3.1\frac{\sigma_{lu}}{f'_{co}}$

the specimens with one and two layers of GTRC exposed to 300 **x2103;**, the strength loss was completely compensated by the index of 1 and 1.13 respectively. Moreover, this index is close to 1 in W-500-2 and W-650-2. In the rest of the specimens including W-500-1 and W-650-1, the repair index is below one, indicating the need for much more considerations such as increasing the number of textile layers, utilizing high strength reinforcing materials or increasing the thickness of confinement mortar.

Additionally, due to the fact that the experimented specimens were not in real size, the severity of damage was higher than that of the real concrete members. So it is expected that the obtained results are also reliable for the real concrete members. However, this needs further investigations.

The typical stress versus axial and hoop strain diagrams at the different regimes of elevated temperature are illustrated in Fig. 12. Axial stress-strain curve for all the specimens initiates with a nearly linear ascending branch. The slope of the linear part is approximately constant for unconfined and confined specimens at the ambient temperature. Within a certain regime of elevated temperature, the ascending slope of the confined specimen's curve is greater than that of the unconfined ones. This trend is much more distinguished in the higher regimes of elevated temperature. Additionally, by increasing the number of confining layers, the slope of the ascending part becomes steeper. In all the confined specimens, the aforementioned ascending branch is followed by an abrupt failure. It seems that the main reason is the brittle behavior of the GTRC composite resulting from the brittleness of AR-glass fibers. There is also a limited number of investigations that reported this abrupt failure in the specimens confined by GTRC [26].

As it can be seen in Fig. 12, the axial strain at peak stress of confined specimens is lower than that of the unconfined

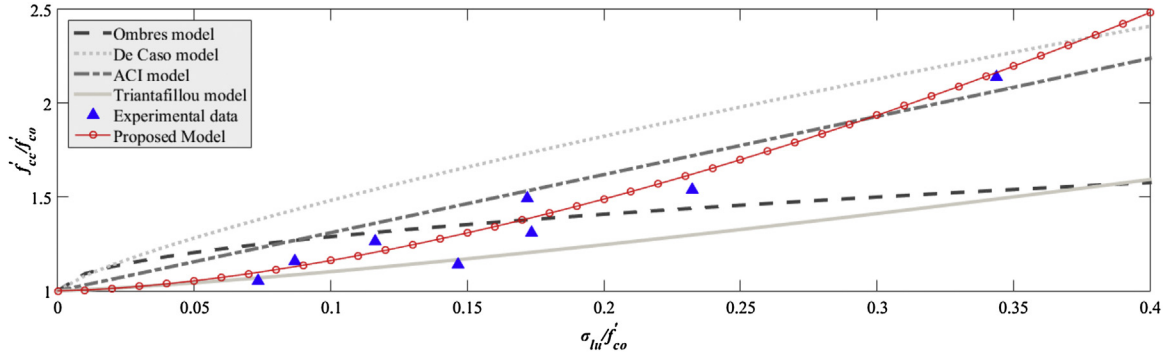

Fig. 14 – Existing prediction models for FRCM-confined concrete beside the proposed experimental model.

specimens in all different temperature regimes. It is also noted that the strain values at peak stress decrease as the number of textile layers increase. This behavior might be attributed to the brittleness of the GTRC composite. Regarding the stress versus hoop strain diagrams in Fig. 12, it can be remarked that there is no meaningful trend in scattered behavior of confined specimens.

The confinement, however, has an incremental effect on the hoop strain at peak stress values compared to unconfined specimens at each thermal regime.

3.3. *Numerical models*

3.3.1. *Simple model for the load-carrying capacity of TRC-confined concrete*

To evaluate the load-bearing capacity of the confined concrete, a simple model was introduced by Ortlepp et al. [51], assuming a rigid bonding between core concrete and TRC jacket. The load-bearing capacity of the confined concrete (F_u) was reported as the maximum of F_{u1} and F_{u2} (Eq. 1).

$$F_u = Max(F_{u1}, F_{u2}) \tag{1}$$

where F_{u1} describes the load-bearing capacity of the confined specimen and is the sum of F_c and F_{fc}, as the load-bearing capacity of the core concrete and confinement layer, respectively (Eq. 2).

$$F_{u1} = F_c + F_{fc} = f'_c \times A_c + 0.27 \times f'_m \times A_m \tag{2}$$

where, f'_c and f'_m are the compressive strength of the core concrete and mortar, respectively. Moreover, A_c refers to the core concrete cross-section area, and A_m is the effective cross-sectional area of fine-grained concrete without textile. The value 0.27 is a reduction factor for fine-grained concrete strength and was obtained based on Ortlepp's et al. study [51]. The second term F_{u2} is as follows (Eq. 3):

$$F_{u2} = f'_c \times A_c \times \left(1 + 0.27 \times \frac{\sigma_{lu}}{f'_c} + 5.55 \times \left(\frac{\sigma_{lu}}{f'_c}\right)^2 - 3.51 \times \left(\frac{\sigma_{lu}}{f'_c}\right)^3 \right) \quad when \quad : \frac{\sigma_{lu}}{f'_{cc}} < 0.8 \tag{3}$$

where, σ_{lu} is ultimate lateral stress imposed by jacketing and is formulated according to Eq. 4.

$$\sigma_{lu} = k_e \frac{(b+d)}{b \times d} \times a_f \times n_{eff} \times f_{fu} \tag{4}$$

With:

a_f : Textile cross-sectional area in one meter of column height

n_{eff} : Number of efficient textile layers

f_{fu} : Tensile strength of the TRC composite

b, d : Geometry of core concrete: Edge length for square columns or diameter in circular columns

k_e : Coefficient of the cross-sectional geometry, which is equal to 1 for circular cross-section

As explained in Ortlepp's et al. study [51], F_{u1} is essentially decisive for the angular cross-section geometries in low reinforcement ratio specimens. In all other cases, the total load capacity F_u is determined by the value of F_{u2}.

For all specimens in this study, F_{u2} is a determinant in total load-bearing capacity estimation. Fig. 13 depicts the comparison between the predicted load-bearing capacity (F_u) and the experimental values, indicating an acceptable agreement for the specimens at the ambient temperature. However, with regards to the effects of elevated temperature on the mechanical properties of the core concrete, as the temperature increases, the predicted values and experimental results diverge from each other, evidently. It seems that further investigations should be taken into account to consider the adverse effects of elevated temperature in the prediction models.

3.2.2. *Compressive strength prediction model for TRC-confined concrete*

According to the available literature, there are various models for predicting the compressive strength of concrete confined by fabric-reinforced cementitious matrixes (FRCM). A number of these models are generally developed based on the assumption that the compressive strength of confined concrete depends on the ultimate lateral stress (σ_{lu}) imposed by the confinement (Eq. 5) [25,29–31]:

$$\frac{f'_{cc}}{f'_{co}} = 1 + \alpha \left(\frac{\sigma_{lu}}{f'_{co}}\right)^{\beta} \tag{5}$$

where α and β are the empirical constants obtained from the experimental data analysis and σ_{lu} has been defined as Eq. 4.

Some of the expressions existing in this field, which predict the compressive strength of the cylindrical concrete specimens confined with FRCM, are summarized in Table 5. These analytical expressions were determined by the experimental investigations, and the contribution of axial strength of the confining jacket to the compressive strength of the FRCM-confined compression member should be neglected [52]. For considering this assumption in our experiments, the 5-mm gaps have been considered on both ends of the specimens to eliminate the potential axial load on the TRC jacket during the tests. As presented in Table 5, the proposed model by Triantafillou et al. predicts the compressive strength of cylindrical specimens confined by carbon fibers. De Caso's et al. model was verified for glass FRCM-confined specimens [53]. Another general model proposed by ACI Committee (549) predicts the peak strength of concrete specimens confined by FRCM [52]. Recently, Ombres and Mazzuca analyzed the results of compression tests on different types of FRCM-wrapped concrete elements to propose a model by means of statistical analysis [54]. Comparing experimental data with the aforementioned models which are plotted in the Fig. 14, reveals no sensible coincidence between experimental data and predicted results. This is potentially due to the effect of elevated temperature on mechanical properties of core concrete that was not considered in these models.

Using a best-fit analysis, a numerical prediction model was proposed based on experimental data derived from the compression test on confined heat-damaged specimens in Eq. 6. Considering the effects of elevated temperature, which is restricted to the regimes reported in this study, Eq. 5 can be rewritten as follows:

$$\frac{f'_{ccT}}{f'_{cT}} = 1 + \alpha\left(\frac{\sigma_{lu}}{f'_{cT}}\right)^{\beta} \tag{6}$$

As it was previously noted, $\boldsymbol{\alpha}$ and $\boldsymbol{\beta}$ are the empirical constants to be calibrated by best-fit analysis. The best-fit analysis revealed that the proposed model with $\boldsymbol{\alpha} = 6.42$ and $\boldsymbol{\beta} = 1.60$, $R^2 = 0.94$, and $RMSE = 0.094$ is formulated as Eq. 7.

$$\frac{f'_{ccT}}{f'_{cT}} = 1 + 6.42\left(\frac{\sigma_{lu}}{f'_{cT}}\right)^{1.60} \tag{7}$$

4. Conclusion

Based on the experimental findings and numerical analysis, the following conclusions can be drawn.

- Comparing experimental results with the predictions of available analytical models for mechanical properties of heat-damaged concrete reveals that the predicted results of models have an acceptable coincidence with the experimental results. Therefore it could demonstrate the accuracy of tests.
- By the preliminary investigation on evaluating the different types of matrixes, it could be concluded that the M3 mortar would be an appropriative choice to confine heat-damaged specimens due to favorable characteristics such as higher ultimate tensile stress, ease of application, and a lower degree of alkalinity of the mixture which could cause the improvement in durability.
- The confinement of specimens by TRC provided a noticeable enhancement in the compressive strength of heat-damaged concrete specimens as well as unheated ones. The more the number of layers applied, the higher the compressive strength and also elastic modulus resulted.
- Regarding the strengthening and retrofitting purposes, this investigation exhibits that TRC could be an appropriate solution for compensating or modulating the strength loss induced by elevated temperature. For specimens exposed to 300 °C, The strength loss is completely compensated by applying only one GTRC layer. Also, the compressive strength of the specimens is compensated after exposure to the 500 °C. It is worth noting that more than approximately 90% of strength loss of the specimens exposed to 650 °C was compensated, which indicates the efficiency of the strengthening method. Obviously, the greater strength loss could be compensated by increasing the number of textile layers, utilizing high strength reinforcing materials, and increasing the thickness of confinement mortar.
- The experimental results of load-bearing capacity and compressive strength enhancement of confined concrete indicate that the predictions of existing models proposed by other researchers are in excellent coincidence with the experimental results at ambient temperature. However, the models' predicted values diverge from experimental results at the elevated temperature, which is mainly attributed to the formation of micro-cracks in core concrete. Accordingly, a numerical model was proposed based on the best-fit analysis to predict the compressive strength of the GTRC-confined heat-damaged concrete exclusively.

Declaration of interests

None.

Acknowledgements

The authors wish to thank appreciatively the Solidian Company, especially Dr. Ali Shams, for their kindly assistance in providing textile sheets.

Appendix A

Nomenclature	
f'_{coT}	Compressive strength of the unconfined concrete at elevated temperature
f'_{cc}	Compressive strength of confined concrete at ambient temperature
f'_{ccT}	Compressive strength of confined heat-damaged concrete
f'_{co}	Compressive strength of unconfined concrete at ambient temperature
f'_{m}	Compressive strength of the mortar
T	Temperature
E_c	Modulus of elasticity of concrete at ambient temperature
E_{cT}	Modulus of elasticity of concrete at elevated temperature
σ_{cT}	Compressive stress induced to concrete at different strain values
σ_{lu}	Ultimate lateral stress due to jacketing
ϵ_{cu}	Axial strain at peak stress at ambient temperature
ϵ_{cuT}	Axial strain at peak stress at elevated temperature
ϵ_{cT}	Strain corresponding
F_u	Load-bearing capacity of the confined concrete
F_c	Load-bearing capacity of the core concrete
F_{fc}	Load-bearing capacity of the confinement layer
A_c	Unconfined concretes cross-section area
A_m	Effective cross-sectional area of mortar without textile
a_f	Cross-sectional area of the textile reinforcement per meter of the column height
f_{fu}	Ultimate tensile strength of the TRC confining composite
k_e	Coefficient for consideration of the cross section geometry
n_{eff}	Effective number of textile layers (without anchorage areas)
b, d	Length of the edge (square) or diameter (circular) of cross-sectional area of the old concrete
α, β	Empirical constant
R^2	Coefficient of determination
RMSE	Root Mean Square Error

Appendix B

Existing numerical models for prediction of mechanical properties of heat-damaged concrete

Mechanical properties	Ref	Model
Compressive strength	EN1992-1-2 [55]	$f'_{coT} = \begin{cases} f'_{co} & \mathbf{T} < \mathbf{100^\circ C} \\ f'_{co}(1.067 - 0.00067\,T) & \mathbf{100^\circ C} \le \mathbf{T} \le \mathbf{400^\circ C} \\ f'_{co}(1.44 - 0.0016\,T) & \mathbf{T} \ge \mathbf{400^\circ C} \end{cases}$
	Kodur et al. [56]	$f'_{coT} = \begin{cases} f'_{co}[1.0625 - 0.003125(T-20)]\,, & \mathbf{T} < \mathbf{100^\circ C} \\ 0.75\,f'_{co}\,, & \mathbf{100^\circ C} \le \mathbf{T} \le \mathbf{400^\circ C} \\ f'_{co}[1.33 - 0.00145\,T]\,, & \mathbf{T} > \mathbf{400^\circ C} \end{cases}$
	Li and Purkiss [57]	$f'_{coT} = f'_{co}\left(0.00165\left(\frac{T}{100}\right)^3 - 0.03\left(\frac{T}{100}\right)^2 + 0.025\left(\frac{T}{100}\right) + 1.002\right)$
	Chang et al. [48]	$f'_{coT} = f'_{co}\left(1.008 + \frac{T}{450\ln\left(T/5800\right)}\right) \ge 0\,,\ \mathbf{20^\circ C} < \mathbf{T} \le \mathbf{800^\circ C}$
Modulus of elasticity	Bastami et al. [58]	$E_{cT} = E_c \begin{cases} 1.0 & \mathbf{20^\circ C} < \mathbf{T} < \mathbf{100^\circ C} \\ 1.015 - 0.00154\,T + 2\times10^{-7}\,T^2 + 3\times10^{-10}\,T^3\,, & \mathbf{100^\circ C} \le \mathbf{T} \le \mathbf{1000^\circ C} \\ 0 & \mathbf{T} > \mathbf{1000^\circ C} \end{cases}$
	Khennane and Baker [59]	$E_{cT} = (-0.001282\,T + 1.025641)E_c\ \mathbf{20^\circ C} \le \mathbf{T} \le \mathbf{800^\circ C}$
	Lu [60]	$E_{cT} = \begin{cases} (1 - 0.0015\,T)E_c & \mathbf{20^\circ C} < \mathbf{T} \le \mathbf{200^\circ C} \\ (0.87 - 0.00084\,T)E_c & \mathbf{200^\circ C} < \mathbf{T} \le \mathbf{700^\circ C} \\ 0.28E_c & \mathbf{T} > \mathbf{700^\circ C} \end{cases}$

(Continued)

Existing numerical models for prediction of mechanical properties of heat-damaged concrete		
	L.W.G. Zhenhai [61]	$E_{cT} = \begin{cases} E_c \; 20^\circ C \le T \le 60^\circ C \\ (0.83 - 0.0011\,T)E_c \; 60^\circ C < T \le 700^\circ C \end{cases}$
Axial strain at peak stress	Bazant and Chern [62]	$\epsilon_{cuT} = \begin{cases} 0.0000064\,T + 0.00216 \; 20^\circ C \le T \le 600^\circ C \\ 0.000015\,T - 0.003 \; 600^\circ C < T \le 650^\circ C \end{cases}$
	Khennane and Baker [59]	$\epsilon_{cuT} = \begin{cases} 0.003 \; 20^\circ C \le T \le 200^\circ C \\ 0.00001156\,T + 0.000686 \le 0.0082 \; T > 200^\circ C \end{cases}$
	Lu [63] and Yao [64]	$\epsilon_{cuT} = \epsilon_{cu}(0.0019\,T + 0.9615)$
	Chang et al. [48]	$\epsilon_{cuT} = \epsilon_{cu} \begin{cases} 1.0 \; 20^\circ C < T \le 200^\circ C \\ \left(-0.1\,f_c' + 7.7\right)\left[\dfrac{exp(-5.8 + 0.01T)}{1 + \exp(-5.8 + 0.01T)} - 0.0219\right] + 1 \; 200^\circ C < T \le 800^\circ C \end{cases}$
Stress-strain relationship	EN1992-1-2 [55]	$\sigma_{cT} = \left[3\epsilon_{cT}\,f_{coT}'/\epsilon_{cuT}\left(2 + \left(\frac{\epsilon_{cT}}{\epsilon_{cuT}}\right)^3\right)\right]$
	Lie and Lin [65]	$\sigma_{cT} = \begin{cases} f_{coT}'\left[1 - ((\epsilon_{cT} - \epsilon_{cuT})/3\epsilon_{cuT})^2\right], \; \epsilon_{cT} > \epsilon_{cuT} \\ f_{coT}'\left[1 - ((\epsilon_{cuT} - \epsilon_{cT})/\epsilon_{cuT})^2\right], \; \epsilon_{cT} \le \epsilon_{cuT} \end{cases}$
	Terro [66]	$\sigma_{cT} = \dfrac{\left(\frac{2f_{coT}'}{\epsilon_{cuT}}\right) \times \epsilon_{cT}}{1 + \left(\frac{\epsilon_{cT}}{\epsilon_{cuT}}\right)^2}$

REFERENCES

[1] J. Ingham, Forensic engineering of fire-damaged structures, Proc. Inst. Civ. Eng. Eng. (2009) 12–17.

[2] W. Inge, S. Nugroho, H. Njo, et al., Strengthening method of concrete structure, in: IOP Conf, Ser. Earth Environ. Sci. (2018), http://dx.doi.org/10.1088/1755-1315/126/1/012051.

[3] T. Trapko, M. Mudisl, The effectiveness of CFRP materials strengthening of eccentrically compressed reinforced concrete columns, Arch. Civ. Mech. Eng. 11 (2011) 249–262. , http://dx.doi.org/10.1016/S1644-9665(12)60187-3.

[4] H. Tran, X. Balandraud, J.F. Destrebecq, I. Pascal, F.- Aubière, Improvement of the mechanical performances of concrete cylinders confined actively or passively by means of SMA wires, Arch. Civ. Mech. Eng. (2014) 4–11. , http://dx.doi.org/10.1016/j.acme.2014.04.009.

[5] A.C.I.C. 440, A.C. Institute, Guide for the Design and Construction of Externally Bonded FRP Systems for Strengthening Concrete Structures, American Concrete Institute, 2008.

[6] CSA. S806-02, Design and Construction of Building Components With Fibrereinforced Polymers, Canadian Standards Association, Mississauga (Canada), 2002.

[7] L.A. Bisby, J.F. Chen, S.Q. Li, T.J. Stratford, N. Cueva, K. Crossling, Strengthening fire-damaged concrete by confinement with fibre-reinforced polymer wraps, Eng. Struct. 33 (2011) 3381–3391. , http://dx.doi.org/10.1016/j.engstruct.2011.07.002.

[8] M. Yaqub, C.G. Bailey, P. Nedwell, Axial capacity of post-heated square columns wrapped with FRP composites, Cem. Concr. Compos. 33 (2011) 694–701. , http://dx.doi.org/10.1016/j.cemconcomp.2011.03.011.

[9] H.S. Al-Nimry, A.M. Ghanem, FRP confinement of heat-damaged circular RC columns, Int. J. Concr. Struct. Mater. 11 (2017) 115–133. , http://dx.doi.org/10.1007/s40069-016-0181-4.

[10] R. Alzeebaree, A. Çevik, B. Nematollahi, J. Sanjayan, Mechanical properties and durability of unconfined and confined geopolymer concrete with fiber reinforced polymers exposed to sulfuric acid, Constr. Build. Mater. 215 (2019) 1015–1032. , http://dx.doi.org/10.1016/j.conbuildmat.2019.04.165.

[11] A. Mohammedameen, M.E. Güls, R. Alzeebaree, A. Çevik, A. Nis, Mechanical and durability performance of FRP confined and unconfined strain hardening cementitious composites exposed to sulfate attack, Constr. Build. Mater. 207 (2019) 158–173. , http://dx.doi.org/10.1016/j.conbuildmat.2019.02.108.

[12] M.E. Gülsan, A. Mohammedameen, M. Sahmaran, A. Nis, R. Alzeebaree, A. Çevik, Effects of Sulphuric Acid on Mechanical and Durability Properties of ECC Confined by FRP Fabrics, Adv. Concr. Constr (2018), http://dx.doi.org/10.12989/acc.2018.6.2.199.

[13] H.R. Hamilton, B. Benmokrane, C.W. Dolan, M.M. Sprinkel, Polymer materials to enhance performance of concrete in civil infrastructure, Polym. Rev. Phila. Pa (Phila Pa) (2009), http://dx.doi.org/10.1080/15583720802656153.

[14] S. Halliwell, FRPs — the environmental agenda, Adv. Struct. Eng. 13 (2010) 783–791. , http://dx.doi.org/10.1260/1369-4332.13.5.783.

[15] T. Triantafillou, Textile Fibre Composites in Civil Engineering, Elsevier Science, 2016.
[16] A. Peled, A. Bentur, B. Mobasher, Textile-reinforced Concrete, Taylor & Francis, 2016.
[17] Y. Du, M. Zhang, F. Zhou, D. Zhu, Experimental study on basalt textile-reinforced concrete under uniaxial tensile loading, Constr. Build. Mater. 138 (2017) 88–100. , http://dx.doi.org/10.1016/j.conbuildmat.2017.01.083.
[18] J. Esmaeili, I. Sharifi, K. Andalibi, J. Kasaei, Effect of different matrix compositions and Micro steel fibers on tensile behavior of textile-reinforced concrete, IOP conf, Ser. Mater. Sci. Eng. 246 (2017), http://dx.doi.org/10.1088/1757-899X/246/1/012031.
[19] Y. Yao, F.A. Silva, M. Butler, V. Mechtcherine, B. Mobasher, Tension stiffening in textile-reinforced concrete under high speed tensile loads, Cem. Concr. Compos. 64 (2015) 49–61. , http://dx.doi.org/10.1016/j.cemconcomp.2015.07.009.
[20] R. Contamine, A.S. Larbi, P. Hamelin, Contribution to direct tensile testing of textile-reinforced concrete (TRC) composites, Mater. Sci. Eng. A. 528 (2011) 8589–8598. , http://dx.doi.org/10.1016/j.msea.2011.08.009.
[21] H.M. Elsanadedy, T.H. Almusallam, S.H. Alsayed, Y.A. Al-Salloum, Flexural strengthening of RC beams using textile-reinforced mortar - Experimental and numerical study, Compos. Struct. 97 (2013) 40–55. , http://dx.doi.org/10.1016/j.compstruct.2012.09.053.
[22] A. Si Larbi, R. Contamine, E. Ferrier, P. Hamelin, Shear strengthening of RC beams with textile-reinforced concrete (TRC) plate, Constr. Build. Mater. 24 (2010) 1928–1936. , http://dx.doi.org/10.1016/j.conbuildmat.2010.04.008.
[23] S.M. Raoof, L.N. Koutas, D.A. Bournas, Textile-reinforced mortar (TRM) versus fibre-reinforced polymers (FRP) in flexural strengthening of RC beams, Constr. Build. Mater. 151 (2017) 279–291. , http://dx.doi.org/10.1016/j.conbuildmat.2017.05.023.
[24] I.M.I. Qeshta, P. Shafigh, M.Z. Jumaat, Research progress on the flexural behaviour of externally bonded RC beams, Arch. Civ. Mech. Eng. 16 (2016) 982–1003. , http://dx.doi.org/10.1016/j.acme.2016.07.002.
[25] T.C. Triantafillou, C.G. Papanicolaou, P. Zissimopoulos, T. Laourdekis, Concrete confinement with textile-reinforced mortar jackets, ACI Struct. J. 103 (2006) 28.
[26] A. Peled, Confinement of damaged and nondamaged structural concrete with FRP and TRC sleeves, J. Compos. Constr. 11 (2007) 514–522. , http://dx.doi.org/10.1061/(ASCE)1090-0268(2007)11:5(514).
[27] R. Ortlepp, A. Lorenz, M. Curbach, Column strengthening with TRC: influences of the column geometry onto the confinement effect, Adv. Mater. Sci. Eng. Int. J. 2009 (2009) 1–6. , http://dx.doi.org/10.1155/2009/493097.
[28] D. García, P. Alonso, J.-T. San-José, L. Garmendia, C. Perlot, Confinement of medium strength concrete cylinders with basalt textile-reinforced mortar, in: 13th Int. Congr. Polym. Concr. [ICPIC 2010]., 2010, 0–7. , http://dx.doi.org/10.1016/j.conbuildmat.2010.12.063.
[29] M. Di Ludovico, A. Prota, G. Manfredi, Structural upgrade using basalt fibers for concrete confinement, J. Compos. Constr. 14 (2010) 541–552. , http://dx.doi.org/10.1061/(ASCE)CC.1943-5614.0000114.
[30] F.J. De Caso y Basalo, F. Matta, A. Nanni, Fiber reinforced cement-based composite system for concrete confinement, Constr. Build. Mater. 32 (2012) 55–65. , http://dx.doi.org/10.1016/j.conbuildmat.2010.12.063.
[31] L. Ombres, S. Mazzuca, Confined concrete elements with cement-based composites: confinement effectiveness and prediction models, J. Compos. Constr. 21 (2016) 4016103, http://dx.doi.org/10.1061/(ASCE)CC.1943-5614.0000755.
[32] R. Ortlepp, S. Ortlepp, Textile-reinforced concrete for strengthening of RC columns: a contribution to resource conservation through the preservation of structures, Constr. Build. Mater. 132 (2017) 150–160. , http://dx.doi.org/10.1016/j.conbuildmat.2016.11.133.
[33] ASTM D 3039/D 3039M, Standard Test Method for Tensile Properties of Polymer Matrix Composite Materials 1, ASTMInternational, WestConshohocken, PA, 2002, http://dx.doi.org/10.1520/D3039_D3039M-17.
[34] B. En, 197-1, Cement-Part 1: composition, specifications and conformity criteria for common cements, Br. Stand. Inst. (2000).
[35] M. Butler, V. Mechtcherine, S. Hempel, Experimental investigations on the durability of fibre–matrix interfaces in textile-reinforced concrete, Cem. Concr. Compos. 31 (2009) 221–231. , http://dx.doi.org/10.1016/j.cemconcomp.2009.02.005.
[36] T. Brockmann, W. Brameshuber, Mechanical and fracture mechanical properties of fine grained concrete for textile-reinforced composites, Fakultät für Bauingenieurwesen (2006).
[37] M. Hinzen, Einfluss Von Kurzfasern auf die Frisch-und Festbetoneigenschaften sowie das Tragverhalten Von Textilbeton, Hochschulbibliothek der Rheinisch-Westfälischen Technischen Hochschule Aachen (2014).
[38] ASTM C109 / C109M-16a, Standard Test Method for Compressive Strength of Hydraulic Cement Mortars (Using 2-in. or [50-mm] Cube Specimens), ASTM International, West Conshohocken, PA, 2016, http://dx.doi.org/10.1520/C0109_C0109M-16A.
[39] ASTM C230 / C230M-14, Standard Specification for Flow Table for Use in Tests of Hydraulic Cement, ASTM International, West Conshohocken, PA, 2014, http://dx.doi.org/10.1520/C0230_C0230M-14.
[40] C. Industry, Assessment, design and repair of fire-damaged concrete structures, Concr. Soc. (2008).
[41] H. Al-Nimry, R. Haddad, S. Afram, M. Abdel-Halim, Effectiveness of advanced composites in repairing heat-damaged RC columns, Mater. Struct. 46 (2013) 1843–1860. , http://dx.doi.org/10.1617/s11527-013-0022-8.
[42] CLG, Approved Document B (Fire Safety) – Volume 2 – Buildings Other Than Dwelling Houses, Department for Communities and Local Government, UK, 2006.
[43] ASTM C39 / C39M-16, Standard Test Method for Compressive Strength of Cylindrical Concrete Specimens, ASTM International, West Conshohocken, PA, 2016, http://dx.doi.org/10.1520/C0039_C0039M-18.
[44] ASTM C469 / C469M-14, Standard Test Method for Static Modulus of Elasticity and Poisson's Ratio of Concrete in Compression, ASTM International, West Conshohocken, PA, 2014, http://dx.doi.org/10.1520/C0469_C0469M-14.
[45] Y.N. Chan, G.F. Peng, M. Anson, Residual strength and pore structure of high-strength concrete and normal strength concrete after exposure to high temperatures, Cem. Concr. Compos. 21 (1999) 23–27. , http://dx.doi.org/10.1016/S0958-9465(98)00034-1.
[46] Q. Ma, R. Guo, Z. Zhao, Z. Lin, K. He, Mechanical properties of concrete at high temperature–a review, Constr. Build. Mater. 93 (2015) 371–383. , http://dx.doi.org/10.1016/j.conbuildmat.2015.05.131.
[47] Y.-F. Fu, Y.-L. Wong, C.-S. Poon, C.-A. Tang, P. Lin, Experimental study of micro/macro crack development and stress–strain relations of cement-based composite materials at elevated temperatures, Cem. Concr. Res. 34 (2004) 789–797. , http://dx.doi.org/10.1016/j.cemconres.2003.08.029.
[48] Y.-F. Chang, Y.-H. Chen, M.-S. Sheu, G.C. Yao, Residual stress–strain relationship for concrete after exposure to high temperatures, Cem. Concr. Res. 36 (2006) 1999–2005. , http://dx.doi.org/10.1016/j.compstruct.2013.10.037.
[49] L. Ombres, Concrete confinement with a cement based high strength composite material, Compos. Struct. 109 (2014) 294–304. , http://dx.doi.org/10.1016/j.compstruct.2013.10.037.

[50] T. Trapko, Confined concrete elements with PBO-FRCM composites, Constr. Build. Mater. 73 (2014) 332–338. , http://dx.doi.org/10.1016/j.conbuildmat.2014.09.055.
[51] R. Ortlepp, M. Curbach, Verstärken Von Stahlbetonstützen mit textilbewehrtem Beton, Beton- Und Stahlbetonbau 104 (2009) 681–689. , http://dx.doi.org/10.1002/best.200900034.
[52] A.C. Institute, ACI 549. 4R-13 Guide to Design and Construction of Externally Bonded Fabric-Reinforced Cementitious Matrix (FRCM) Systems for Repair and Strengthening Concrete and Masonry Structures, American Concrete Institute, 2014.
[53] F.J. De Caso Y Basalo, F. Matta, A. Nanni, Fiber reinforced cement-based composite system for concrete confinement, Constr. Build. Mater. 32 (2012) 55–65. , http://dx.doi.org/10.1016/j.conbuildmat.2010.12.063.
[54] L. Ombres, S. Mazzuca, Confined concrete elements with cement-based composites: confinement effectiveness and prediction models, J. Compos. Constr. 21 (2016) 4016103, http://dx.doi.org/10.1061/(ASCE)CC.1943-5614.0000755.
[55] CEN- European Committee for Standardization, EN 1992-1-2: Design of Concrete Structures - Part 1-2: General Rules - Structural Fire Design, Des. Concr. Struct. - Part 1-2 Gen. Rules-Structural Fire Des. 2 (2004) 1–99.
[56] V.K.R. Kodur, T.C. Wang, F.P. Cheng, Predicting the fire resistance behaviour of high strength concrete columns, Cem. Concr. Compos. 26 (2004) 141–153. , http://dx.doi.org/10.1016/S0958-9465(03)00089-1.
[57] L.Y. Li, J. Purkiss, Stress-strain constitutive equations of concrete material at elevated temperatures, Fire Saf. J. 40 (2005) 669–686. , http://dx.doi.org/10.1016/j.firesaf.2005.06.003.
[58] M. Bastami, F. Aslani, O.M. ESMAEILNIA, High-temperature mechanical properties of concrete, Int. J. Civ. Eng. 8 (2010) 337–351.
[59] A. Khennane, G. Baker, Uniaxial model for concretee under variable temperature and stress, J. Eng. Mech. 119 (1994) 1507–1525. , http://dx.doi.org/10.1061/(ASCE)0733-9399(1993)119:8(1507).
[60] B. Yu, Fire Response of Reinforced Concrete Beams Strengthened With Near-surface Mounted FRP Reinforcement, Michigan State University, 2013.
[61] L.W.G. Zhenhai, Experimental investigation of strength and deformation of concrete at elevated temperature, J. Build. Struct. 1 (1993) 1.
[62] Z.P. Bažant, J.-C. Chern, Stress-induced thermal and shrinkage strains in concrete, J. Eng. Mech. 113 (1987) 1493–1511.
[63] Z.-D. Lu, A Research on Fire Response of Reinforced Concrete Beams, Tongji Univ., 1989.
[64] Y.X. Yao, Research on Fire Response of Reinforced Concrete Frames and Determination of Temperature Reached During a Fire, Tongji Univ., 1991.
[65] T.T. Lie, T.D. Lin, Fire performance of reinforced concrete columns, in: Fire Saf. Sci. Eng., ASTM International, 1985.
[66] M.J. Terro, Numerical modeling of the behavior of concrete structures in fire, ACI Struct. J. 95 (1998), http://dx.doi.org/10.14359/538.